Amino Acids (2010) 39:59–71
DOI 10.1007/s00726-009-0364-2

ORIGINAL ARTICLE

Structural analysis of the complex between calmodulin and full-length myelin basic protein, an intrinsically disordered molecule

Viivi Majava · Chaozhan Wang · Matti Myllykoski · Salla M. Kangas · Sung Ung Kang · Nobuhiro Hayashi · Peter Baumgärtel · Anthony M. Heape · Gert Lubec · Petri Kursula

Received: 15 September 2009 / Accepted: 7 October 2009 / Published online: 24 October 2009

Abstract Myelin basic protein (MBP) is present between the cytoplasmic leaflets of the compact myelin membrane in both the peripheral and central nervous systems, and characterized to be intrinsically disordered in solution. One of the best-characterized protein ligands for MBP is calmodulin (CaM), a highly acidic calcium sensor. We pulled down MBP from human brain white matter as the major calcium-dependent CaM-binding protein. We then used full-length brain MBP, and a peptide from rodent MBP, to structurally characterize the MBP–CaM complex in solution by small-angle X-ray scattering, NMR spectroscopy, synchrotron radiation circular dichroism spectroscopy, and size exclusion chromatography. We determined 3D structures for the full-length protein–protein complex at different stoichiometries and detect ligand-induced folding of MBP. We also obtained thermodynamic data for the two CaM-binding sites of MBP, indicating that CaM does not collapse upon binding to MBP, and show that CaM and MBP colocalize in myelin sheaths. In addition, we analyzed the post-translational modifications of rat brain MBP, identifying a novel MBP modification, glucosylation. Our results provide a detailed picture of the MBP–CaM interaction, including a 3D model of the complex between full-length proteins.

Keywords Myelin · Calmodulin · Protein complex · 3-dimensional structure · Myelin basic protein · Proteomics

V. Majava and C. Wang contributed equally to this work.

Electronic supplementary material The online version of this article (doi:10.1007/s00726-009-0364-2) contains supplementary material, which is available to authorized users.

V. Majava · C. Wang · M. Myllykoski · P. Kursula (✉)
Department of Biochemistry, University of Oulu,
PO Box 3000, 90014 Oulu, Finland
e-mail: petri.kursula@oulu.fi

S. M. Kangas · A. M. Heape
Department of Anatomy and Cell Biology,
Institute of Biomedicine, University of Oulu, Oulu, Finland

S. U. Kang · G. Lubec
Department of Pediatrics, Medical University of Vienna,
Vienna, Austria

N. Hayashi
Department of Life Science, Tokyo Institute of Technology,
Tokyo, Japan

P. Baumgärtel
Department of Physical Biochemistry,
University of Potsdam, Potsdam, Germany

P. Baumgärtel
Helmholtz-Zentrum Berlin, BESSY II, Berlin, Germany

Abbreviations

CaM	Calmodulin
MBP	Myelin basic protein
MPE	Myelin protein extract
SAXS	Small-angle X-ray scattering
bMBP	Bovine MBP
pMBP	Porcine MBP
mMBP	Mouse MBP
SRCD	Synchrotron radiation circular dichroism spectroscopy
PTM	Post-translational modification
3DE	3-Dimensional electrophoresis
IDP	Intrinsically disordered protein
SC	Schwann cell
DRG	Dorsal root ganglion
MM	Molecular mass

SPR	Surface plasmon resonance
ITC	Isothermal titration calorimetry
PNS	Peripheral nervous system
CNS	Central nervous system
RT	Room temperature
FCS	Fetal calf serum
SL	Schmidt–Lanterman incisure
CM	Compact myelin
ΔC_p	Heat capacity

Introduction

Myelin, the insulating, multi-layered membrane structure surrounding an axon, provides an increase in the speed of nerve impulses; thus, it is essential for proper functioning of the vertebrate nervous system. Myelin is mainly composed of lipid and protein, the latter constituting 20% of its dry weight. The two most abundant proteins in central nervous system (CNS) myelin are the proteolipid protein and the myelin basic protein (MBP); they represent 50 and 30%, respectively, of the total myelin protein (Benjamins and Morell 1978). MBP is also an abundant component of peripheral nervous system (PNS) myelin (Garbay et al. 2000).

The MBP family comprises numerous developmentally regulated isoforms, of which the 18.5-kDa species is the most abundant in adult human myelin, and has been studied the most (Bates et al. 2000; Homchaudhuri et al. 2009; Polverini et al. 2008; Zhong et al. 2007). This isoform further undergoes complex posttranslational modifications (PTM), giving rise to charge isomers designated as components C1–C8 (Zand et al. 1998), of which C1 is the least modified form (Hill and Harauz 2005). MBP is one of the major autoantigens in multiple sclerosis, which has led to a number of studies on its disease-linked epitopes and their structure (Kim et al. 2003; Spyranti et al. 2009; Tselios et al. 1998).

MBP is essential for the formation of CNS myelin, and it is able to interact with a wide range of ligands, often polyanionic in nature (Boggs 2006), including, for example, cytoskeletal proteins (Barylko and Dobrowolski 1984; Boggs 2006; Boggs and Rangaraj 2000; Dobrowolski et al. 1986; Hill and Harauz 2005). Due to the large number of charged residues and a low overall hydrophobicity, there is significant intramolecular electrostatic repulsion in MBP; this results in MBP being an extended, intrinsically disordered protein (IDP) in solution (Harauz et al. 2004), and it displays the general properties of an IDP in the absence of bound ligands. Usually, an IDP has sufficient flexibility to bind various charged surfaces and ligands and to acquire local conformations necessary to optimize its specific binding to different targets (Dyson and Wright 2002).

Various techniques have been used to prove that the 18.5-kDa isoform of MBP can interact with calmodulin (CaM) (Libich and Harauz 2002a; Libich and Harauz 2002b; Libich et al. 2003a; Libich et al. 2003b; Majava et al. 2008b). MBP is bound to CaM at a 1:1 ratio under near-physiological conditions (Libich et al. 2003a), but it has also been reported that MBP has multiple CaM-binding sites (Libich et al. 2003b). Recently, NMR studies of full-length recombinant 18.5-kDa MBP binding to CaM (Libich and Harauz 2008), with the goal of definitively identifying the primary CaM interaction site on murine MBP, were carried out. The data currently available support a scenario, in which MBP interacts with CaM primarily via its C-terminal site (Libich and Harauz 2008; Majava et al. 2008b). However, more data are needed to gain a comprehensive understanding of the interactions.

Despite the fact that myelin proteins have been studied for decades, little structural information is still available on them or the complexes they form with other molecules (Kursula 2008). Here, the interaction between CaM and full-length MBP from brain is studied using affinity and gel filtration chromatography, surface plasmon resonance (SPR), isothermal titration calorimetry (ITC), as well as proteomics and cell biological methods, in order to gain further insights into the interactions between the full-length proteins. Small-angle X-ray scattering (SAXS), NMR spectroscopy, and synchrotron radiation circular dichroism (SRCD) spectroscopy are also applied to provide 3D structural information of the complex.

Materials and methods

Proteins and peptides

MBP from pig, mouse, and bovine brain (pMBP, mMBP, and bMBP, respectively) was purchased from Fermlabs (Turku, Finland). The preparation is obtained by a chloroform extraction method (Maatta et al. 1997), and mainly contains the 18.5-kDa isoform (Majava et al. 2008b). Vertebrate full-length CaM was purified as described previously (Kursula and Majava 2007). A peptide representing the C-terminal CaM binding site from mMBP (HKGFKGAYDAQGTLSKIFK; residues 136–154 of MBP) was purchased from SBS Genetech (China); the N and C termini were acetylated and amidated, respectively.

Calmodulin affinity pulldown

Human brain samples were obtained during autopsy (Department of Pathology, Oulu Central Hospital, Finland). Permission to use human brain tissue for research was obtained from the Finnish Medico-Legal Council

(permit 102/32/200/99). Blocks of ~2 cm^3 of white matter were dissected from the cerebral hemispheres of an 89-year-old male patient, with no known neurological diseases, and stored at −20°C in 1 mM EDTA.

For affinity chromatography, a block of white matter was homogenized in 10 ml of lysis buffer (10 mM HEPES, pH 7.5, 100 mM NaCl, 0.1% Triton X-100, 10 mM $CaCl_2$) with EDTA-free Complete protease inhibitors (Roche), using a glass-teflon homogenizer on ice. The lysate was clarified by centrifugation at 27,000*g* for 20 min at +4°C. 1 ml of CaM agarose (Sigma) was equilibrated using the lysis buffer, and mixed with 5 ml of the lysate at +4°C for 1 h. The mixture was poured into a column and allowed to drain. The matrix was washed with the lysis buffer until no more protein eluted (15 × 1 ml). Elution (10 mM HEPES pH 7.5, 100 mM NaCl, 10 mM EDTA) was carried out collecting 1-ml fractions.

The samples were analyzed by SDS-PAGE and Coomassie staining, and proteins were identified by tryptic peptide mapping at the Proteomics Core Facility of Biocenter Oulu.

Size exclusion chromatography

A Superdex 75 HR 10/30 column was operated by the ÄKTA *purifier* system (GE Healthcare) using 20 mM HEPES pH 7.5, 100 mM NaCl, 20 mM $CaCl_2$ as a running buffer, at a flow rate of 0.5 ml/min. Size exclusion chromatography was done for 500-µl samples of 50 µM bMBP and 50 µM CaM separately, and for complexes mixed with bMBP:CaM ratios of 1:1, 1:2, and 1:5 (25:25, 25:50, and 25:125 µM, respectively). Mixtures of globular proteins of known molecular mass (MM) were similarly run through the column for calibration.

Surface plasmon resonance

The binding of pMBP to immobilized CaM was studied by SPR using the Biacore 3000 apparatus (GE Healthcare) at +25°C. CaM was immobilized onto a CM5 chip (GE Healthcare) as previously described (Majava et al. 2008b). Dilutions of pMBP were made in the SPR buffer (20 mM HEPES pH 7.5, 100 mM NaCl, 10 mM $CaCl_2$, 0.004% surfactant P-20). During the run, a flow rate of 10 µl/min was used, and duplicate 30-µl injections were made at each concentration. The data were analyzed using GraphPad Prism.

Isothermal titration calorimetry

ITC was used to analyze the binding of CaM both to the mMBP peptide and to full-length pMBP and bMBP, using the MicroCal VP-ITC (Microcal Inc). CaM and bMBP were dialyzed against 100 mM HEPES pH 7.5, 20 mM $CaCl_2$. bMBP (2.5 µM) was titrated with 10-µl injections of CaM (50 µM), at +20, +25, +30, and +35°C. The CaM–bMBP interaction was also analyzed in the reverse manner, i.e., with bMBP in the syringe and CaM in the measurement cell, at +20 and +25°C.

ITC for CaM binding to pMBP and the mMBP peptide was carried out similarly, with the following exceptions: The samples were dialyzed into 20 mM HEPES pH 7.5, 100 mM NaCl, 10 mM $CaCl_2$. The concentrations used in the peptide complex titration were 8 µM for CaM and 240 µM for the peptide, and in the pMBP/CaM titration 11 µM for pMBP and 160 µM for CaM. The titration was carried out at +20 and +25°C (peptide) and +30°C (pMBP) with injection volumes of 15 µl. The ITC data were analyzed with MicroCal Origin (MicroCal).

Small-angle X-ray scattering

Synchrotron SAXS data for CaM, pMBP, and the respective complex at 1:1 and 1:2 MBP:CaM ratios were collected on beamline I711 at MAX-Lab, Lund, Sweden (Cerenius et al. 2000). In addition, data were collected on the complex between CaM and the mMBP peptide. All samples were dialyzed against the assay buffer (20 mM HEPES pH 7.5, 100 mM NaCl, 10 mM $CaCl_2$). An exposure time of 10 min was used. Data were processed using the in-house Bli711 software at MAX-Lab, and ATSAS (Konarev et al. 2006) was used for further data analysis and molecular modeling, as previously described (Majava et al. 2008b).

NMR spectroscopy

Stable isotope labeled CaM was prepared, and all NMR experiments were carried out, as previously described (Majava et al. 2008b). The assignments for the nuclei of CaM were achieved previously (Majava et al. 2008b). The assignments for the protein backbone nuclei of the ^{15}N-labeled CaM–MBP complex were achieved by the two-dimensional ^{1}H-^{15}N HSQC spectral changes induced by titrations of MBP to CaM.

Synchrotron radiation CD spectroscopy

As a synchrotron light source for SRCD (Sutherland 1996), we used the dipole beamline D12.2-3mNIM-C at BESSY II (Reichardt et al. 2001). A LiF window (Korth Kristalle GmbH, Altenholz, Germany) separates the ultra-high vacuum of the beamline from the experimental chamber under atmospheric pressure. As the pressure difference introduces stress strain birefringence in the LiF window, a MgF_2 Rochon polarizer (B. Halle Nachfl. GmbH, Berlin, Germany) follows in the optical path, ensuring linear

polarization. A photo-elastic modulator (PEM) (Hinds Instruments, Hillsboro, USA; model I/CF50) for converting the linearly polarized light into modulated circularly polarized light was used. The sample was placed in the focus of the beam, which had horizontal and vertical dimensions (full width at half maximum) of 1 ± 0.1 and 2 ± 0.1 mm, respectively. The photon flux at this position is about 1×10^{11} photons/s at a bandwidth of 1 nm. The PEM was calibrated (Oakberg et al. 2000), and the absolute CD sensitivity was verified by calibrating with (+)-10-camphorsulfonic acid.

SRCD data were collected on pMBP (0.6 mg/ml), CaM (0.9 mg/ml), and their complex at ratios of 1:1 (0.49:0.45 mg/ml) and 1:2 (0.49:0.9 mg/ml). The samples were dialyzed into 10 mM KPO4 (pH 7.6), and $CaCl_2$ was added to 2 mM immediately prior to measurement. Data were also collected for samples of pMBP titrated with different concentrations of Zn acetate (in this case, $CaCl_2$ was not added to the dialyzed sample). A rectangular 10- or 100-μm quartz cuvette was used (Hellma, Müllheim, Germany). Data processing and analysis were carried out in IgorPro (WaveMetrics, Lake Oswego, Oregon, USA), using a local extension for SRCD data. Each spectrum is the baseline corrected average of three successive scans of the sample with a stepwise scan rate of 3 s/nm.

Proteomics methods

The preparation of myelin protein extracts (MPE), 3D gel electrophoresis (3DE), in-gel digestion, and protein and PTM identification were carried out essentially as described earlier (Baer et al. 2009; Majava et al. 2008a). Detailed protocols are given as supplementary information.

Immunocytochemical methods

Mice

Mice (CD-1 strain) were from the Laboratory Animal Centre (University of Oulu), and the Animal Welfare Committee approved their use and the protocols (permit number 035/07).

Antibodies

Primary antibodies were polyclonal rabbit anti-MBP (Garbay et al. 1988) and monoclonal mouse anti-CaM Ab-4 (NeoMarkers). Secondary antibodies (Molecular Probes) were Alexa Fluor 568 goat anti-rabbit IgG (H + L) and Alexa Fluor 488 goat anti-mouse IgG (H + L).

Cell culture

The isolation, purification, and expansion of myelination-competent Schwann cells (SC) from 4-day-old mouse pups (Honkanen et al. 2007), and the purification and culture of mouse dorsal root ganglion (DRG) sensory neurons from 14.5-day-old mouse embryos on three-dimensional Matrigel^{TM}-coated glass coverslips (Päiväläinen et al. 2008), have been described previously. Myelinating mouse SC/DRG neuron cocultures were performed as described (Päiväläinen et al. 2008), using 30,000 SCs and 2 DRGs for each coculture. Myelination was allowed to proceed for 3 weeks, when myelin sheaths were clearly visible by phase-contrast microscopy.

Immunocytochemistry

The cocultures were rinsed three times with PBS, fixed with 2.5% paraformaldehyde in PBS for 10 min at room temperature (RT), permeabilized for 6 min with ice-cold methanol, and blocked with 1.5% fetal calf serum (FCS) in PBS for 1 h at room temperature (RT). Simultaneous incubation with the anti-MBP and anti-CaM primary antibodies, at final respective dilutions of 1:150 and 1:100 in PBS containing 1.5% FCS, was carried out overnight at +4°C, followed by three 10-min washes with PBS. Simultaneous incubation with goat-anti-mouse and goat-anti-rabbit secondary antibodies, at final respective dilutions of 1:150 and 1:200 in PBS containing 1.5% FCS, was carried out for 2 h at RT, followed by two 10-min washes with PBS. Cell nuclei were stained with 0.2 μg/ml Hoechst nucleus dye (Sigma) in PBS for 10 min at RT, washed twice with PBS for 10 min, twice with sterile H_2O, and the coverslips were mounted on microscope slides.

Microscopy

The cultures were routinely checked using a LeicaDMIL phase-contrast microscope. Immunofluorescence confocal microscopy of the myelinating cocultures was carried out with a Zeiss LSM 510 Laser Scanning microscope equipped with Argon (488 nm) and HeNe (excitation 543 nm) lasers, using a 100× oil immersion objective (Plan-Apochromat 100×/1.4 oil DIC). Images of 11–16 0.2-μm optical slices (vertical *Z*-axis) were made for each field.

Results

MBP from human brain white matter binds to calmodulin

CaM-binding proteins from human brain white matter were analyzed using calcium-dependent CaM pulldown and subsequent tryptic peptide mapping of the detected proteins. Out of the five strongest Coomassie-stained bands from SDS-PAGE (Fig. 1a), four were identified as MBP;

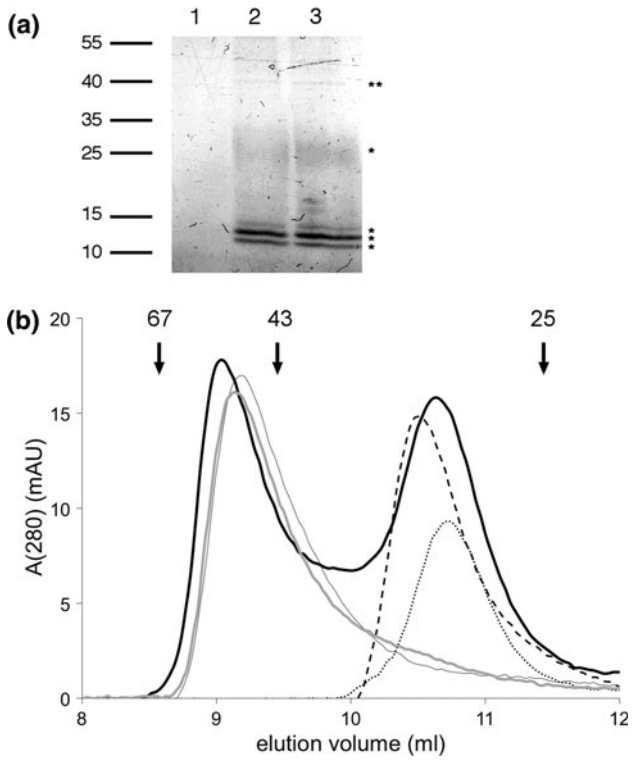

Fig. 1 Initial binding analyses for MBP and CaM. **a** CaM pulldown analysis of human post-mortem brain white matter. The samples are the first three eluates from the affinity column after washing. The positions of MM markers (in kDa) are shown on the *left*, and the *asterisks* denote MBP (*) and MAPK (**). **b** Size exclusion chromatography of the bMBP–CaM complex. Positions of MM markers (in kDa) are shown above the graph. The void volume of the column is approximately 7.2 ml. The samples are MBP (*dashed line*), CaM (*dotted line*), MBP:CaM 1:1 (*thin line*), MBP:CaM 1:2 (*thick gray line*), and MBP:CaM 1:5 (*thick black line*). Note the excess CaM in the 1:5 sample

the 40-kDa protein was identified as a MAP kinase. Thus, MBP is a quantitatively major CaM-binding protein in human brain white matter, when a lysate is prepared in the presence of a mild detergent, 0.1% Triton X-100.

Analysis of the MBP-CaM complex by size exclusion chromatography

The complex between bMBP and CaM at different stoichiometric ratios was analyzed by size exclusion chromatography (Fig. 1b). CaM (17 kDa) is dumbbell-shaped and MBP (18.5 kDa) unfolded; thus, their elution volume corresponds to an apparent MM of 30 kDa. The elution volumes of the complex in the samples with molecular ratios of 1:1, 1:2 and 1:5 are close to each other, corresponding to an apparent MM of 50 kDa. In the 1:5 sample, excess CaM not present in the complex eluted as a separate peak. In the 1:1 and 1:2 complexes, no peak indicating the presence of uncomplexed CaM is seen. Hence, all CaM in these samples is present in the complex with MBP, proving 1:2 complex formation.

From the elution volumes, it can be seen that the hydrodynamic radius ('apparent MM') of the MBP–CaM complex only exhibits minor differences between the 1:1 and 1:2 stoichiometries. Due to the expected non-globular nature of both MBP, CaM, and their respective complexes at different stoichiometric ratios, no direct conclusions can be made about the MM of the complexes based on size exclusion chromatography; mobility depends on both size and shape of the particle, i.e., the hydrodynamic radius.

Full-length MBP has two binding sites for CaM with sub-micromolar affinity

We studied the interaction of CaM with MBP by ITC (Fig. 2, Table 1). The experiment was performed with bMBP, pMBP, and a peptide from mMBP. bMBP was analyzed in most detail, including a temperature series; ΔH was plotted against temperature to obtain the heat capacity (ΔC_p) for the two CaM-binding sites in bMBP. ΔC_p can be used to estimate the surface area buried upon complex formation. ΔC_p for both binding sites is approximately -200 cal/molK, indicating that CaM does not collapse around its binding sites on MBP (in which case, $\Delta C_p \approx -800$ cal/molK would be expected (Brokx et al. 2001)), and that the buried surface area is likely to be rather small, possibly involving many electrostatic interactions.

When MBP was present in the measurement cell and CaM in the syringe, two separate binding sites with different affinity were clearly detected with both bMBP and pMBP, and thermodynamic parameters could be determined for both sites. The affinity for the weaker site was in the 0.1–1 μM range, while the higher-affinity site had $K_d \approx 10$ nM (Table 1). When CaM was in the cell and bMBP in the syringe, the two binding sites are less easy to distinguish, since first, in excess CaM, a 1:2 complex is formed, and thus, the titration curve will include a component related to the dissociation of CaM from the weaker binding site. To complement the ITC assays, SPR analysis of the pMBP binding to immobilized CaM was carried out; the observed K_d was 148 ± 17 nM (Fig. 2c).

The C-terminal region of MBP is assumed to be the main binding site for CaM; previously, we studied a peptide from this region in hMBP (Majava et al. 2008b). Here, we additionally analyzed a corresponding peptide from mMBP. The peptide bound CaM with an affinity in the 10 μM range, i.e., significantly weaker than the full-length protein. The heat capacity is in the range of -500 cal/molK, which is indicative of the peptide interacting mainly with one lobe of CaM (Brokx et al. 2001).

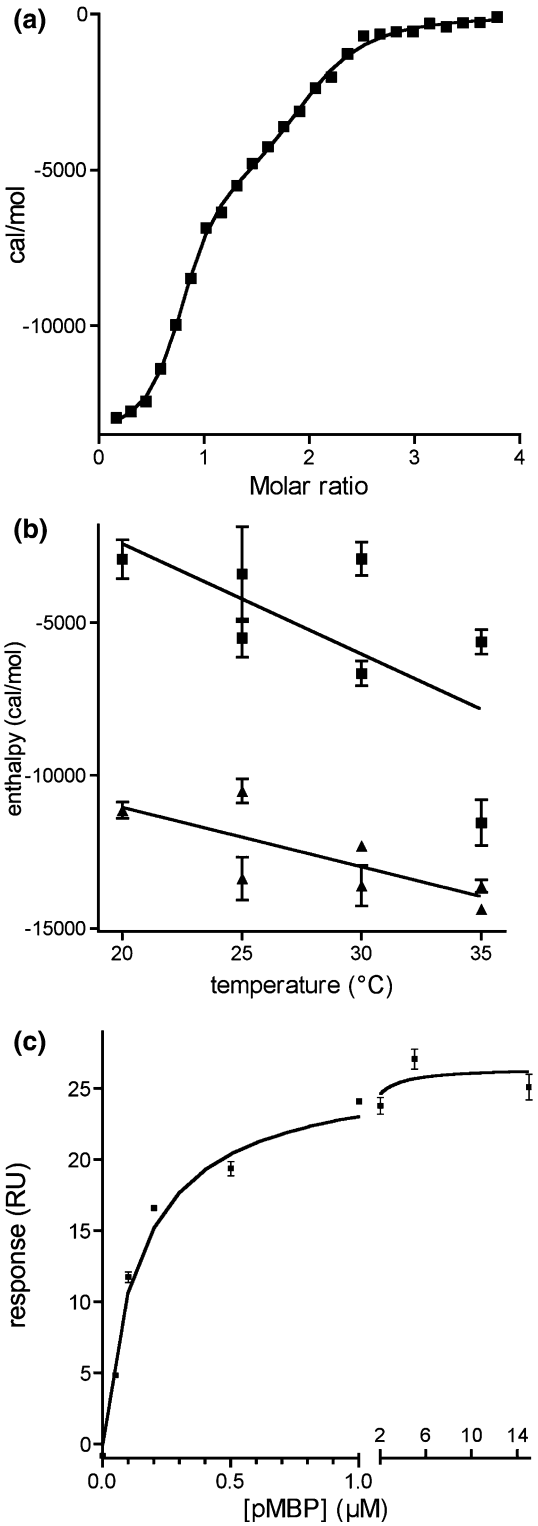

◀ **Fig. 2** Analysis of the MBP–CaM interaction by calorimetry and surface plasmon resonance. **a** ITC titration of CaM into bMBP at +35°C; the two binding sites are clearly detectable. The points indicate raw titration data, and the line shows the fit to a 2-site binding model. **b** The binding enthalpy for the CaM–bMBP complex as a function of temperature. Each experiment for the two binding sites has been plotted separately; the slope of the linear fit gives an approximation of the heat capacity. Triangles, high-affinity site; squares, low-affinity site. c. SPR analysis of pMBP binding to immobilized CaM

Solution structures of CaM complexed to full-length MBP and an MBP peptide

We used synchrotron SAXS to analyze the 3D solution structures of the complexes between CaM and full-length pMBP or the mMBP peptide (Fig. 3, Table 2). Taking CaM as the reference, MMs of the complexes were estimated from forward scattering, $I(0)$, and excluded volume of the ab initio model, V_p. The MM of the 1:2 complex calculated from $I(0)$ is very close to that expected; thus, the molar ratio of MBP to CaM in the complex is really 1:2. The 1:1 complex mixture partially precipitated upon complex formation, followed by apparent resolubilization; however, the $I(0)$ indicates that some protein was lost. Comparing the V_p of the 1:1 and 1:2 complexes, their ratio is 1.5, exactly as expected. This implies that the 1:1 mixture is also in a complex form, being much larger than CaM or MBP, but smaller than the 1:2 complex. Both of the MBP–CaM complexes—1:1 and 1:2—have nearly the same radius of gyration; furthermore, the maximum diameters of the two complexes are similar to unfolded pMBP (Table 2), suggesting that MBP remains extended in the complexes. The distance distributions (Fig. 3b) indicate that the 1:1 and 1:2 complexes have distinct conformations in solution.

Table 1 Calorimetric data

Sample	T (°C)	n	ΔH (kcal/mol)	K_d
pMBP	30	0.9	−2.6	1.6 μM
		0.4	−6.6	85 nM
mMBP peptide	25	1.1	−10.9	12 μM
	20	1.1	−8.3	10 μM
bMBP	20	1.2	−2.9	99 nM
		1.2	−11.1	7 nM
	25	0.9	−4.5	131 nM
		1.2	−11.9	6 nM
	30	1.3	−4.8	310 nM
		0.7	−13.0	10 nM
	35	1.2	−8.6	715 nM
		0.7	−14.0	19 nM
bMBP (reverse)	20	0.5	−26.8	184 nM
	25	0.5	−34.8	410 nM

The data are shown for two binding sites, except for the peptide and the reverse titration with bMBP, for which fitting was done with one binding site

For the titrations with bMBP, the mean from two experiments is given. All enthalpy data points are shown in Fig. 2b

The IDP nature of MBP is shown by the Kratky plot (Fig. 3c), in which no maximum characteristic of a folded protein is seen. In line with this, model building results in a highly elongated unfolded molecule; such behavior of MBP in aqueous solution is well-characterized (Chao and Einstein 1970). Ab initio models of the pMBP–CaM complexes (Fig. 3d) provide a 3D insight into the complex formation between these two full-length proteins. The 1:1 complex is elongated, with a CaM-sized density present close to one end of the shape. In the 1:2 complex, the maximum dimension remains nearly unaltered, but the shape becomes thicker, with a second CaM molecule bound towards the other end. This is in line with earlier predictions and experimental results (Harauz and Libich 2009; Libich et al. 2004).

The CaM-mMBP peptide complex was also analyzed by SAXS (Fig. 3e, Table 2); the radius of gyration decreased by approximately 2 Å in the presence of the peptide, and the maximum diameter by 0.5 nm. At the same time, the apparent MM showed a slight increase. The complex is slightly more compact than unliganded CaM; however, it is not as compact as a complex with a fully collapsed conformation of CaM. Ab initio molecular modeling (Fig. 3d) also shows that CaM remains in an extended conformation, and the peptide binds between the two lobes of CaM. The results are similar to those obtained using the corresponding peptide from hMBP (Majava et al. 2008b), although the current complex is slightly more compact. While this region in MBP has been characterized as the main CaM binding site (Libich et al. 2003a; Libich et al. 2003b), depending on the species, there is a 1-residue insertion within this sequence when compared to hMBP. The results indicate that the sequence differences in this region between species may have small effects on CaM binding, but do not significantly affect complex formation.

NMR analysis of the MBP–CaM complex

NMR spectroscopy was used to identify CaM residues, whose chemical shifts changed upon binding MBP (Fig. 4). Although the reduction of signal intensities resulting from complex formation made the analyses difficult, relevant information was obtained. The residues with changes in chemical shifts are mostly concentrated around the hydrophobic pocket of the CaM C-terminal lobe; identified residues include Arg106, Leu116, Gly134, Val136, Gly140, Ala147, and Lys148. The fact that chemical shift perturbations were also observed for residues in the central helix indicates either bending of the helix upon MBP binding or a direct interaction between MBP and the central helix. The chemical shift perturbations of some residues, mainly Gly25 and Thr26, of the N-terminal lobe further suggest that MBP interacts also weakly with the N-terminal lobe. Taken together, the NMR data show that MBP interacts mainly with the CaM C-terminal lobe, but also with the central helix and the N-terminal lobe. These results are consistent with those obtained using recombinant mMBP (Libich and Harauz 2008) and a human MBP peptide (Majava et al. 2008b).

Evidence for ligand-induced folding of MBP

SRCD was used to analyze CaM, pMBP, and their complex at different stoichiometric ratios (Fig. 5a). As expected, the spectra for CaM and pMBP alone indicate mainly helical and random coil structures, respectively (data not shown). A comparison of the spectra for the complexes shows that for the complexes, the spectrum is approximately that obtained by a simple summation of the individual spectra for pMBP and CaM. Thus, either MBP presents no changes in secondary structure content upon CaM binding, or when the complex is formed, CaM loses some of its secondary structure simultaneously.

To further analyze the possibility of ligand-induced folding of MBP, SRCD spectra were also measured for pMBP at different concentrations of Zn^{2+} (Fig. 5b), in potassium phosphate buffer. When Zn^{2+} concentration reaches a threshold, it induces the folding of pMBP. At the same time, pMBP becomes very sticky, e.g., binding to the cuvette (data not shown).

Post-translational modifications of rat brain MBP

MPEs from rat brain were prepared and analyzed by 3DE (Supplementary Fig. 1). 15 spots representing MBP were picked and analyzed for the presence of PTMs (Supplementary Table 1); some of the detected modifications have not previously been characterized, such as the glucosylation of Asn82 and Asn90 (numbering for the 18.5-kDa form), while others are well-known (Kim et al. 2003), including Gln119 deamidation and two phosphorylation sites, Ser68 and Thr96. PTMs were observed in the predicted central CaM-binding site and in its vicinity; these modifications include phosphothreonine 96 and the two glucosylation sites. No citrullination was detected in any of the spots, despite citrullination being a common modification of MBP. The presence of CaM in the MPE was also confirmed by mass spectrometry using similar methods (Supplementary Fig. 2; Supplementary Table 2).

Colocalization of MBP and CaM in cultured myelin

SC/DRG cocultures that have been under myelination-promoting conditions for 3 weeks contain SCs at all stages of differentiation. These range from the establishment of contact with neurons, in which MBP expression is weak,

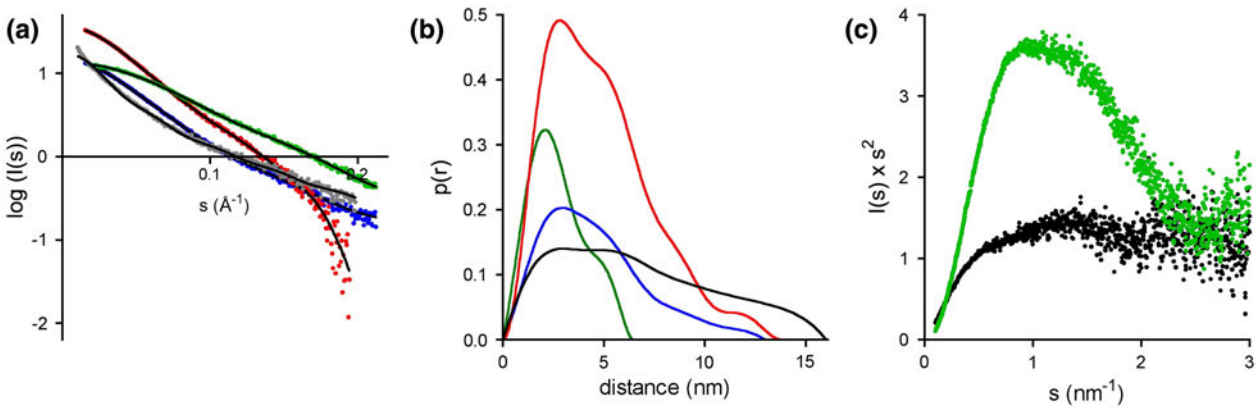
(a)
log (I(s))
s (Å^{-1})
(b)
p(r)
distance (nm)
(c)
I(s) x s^2
s (nm^{-1})

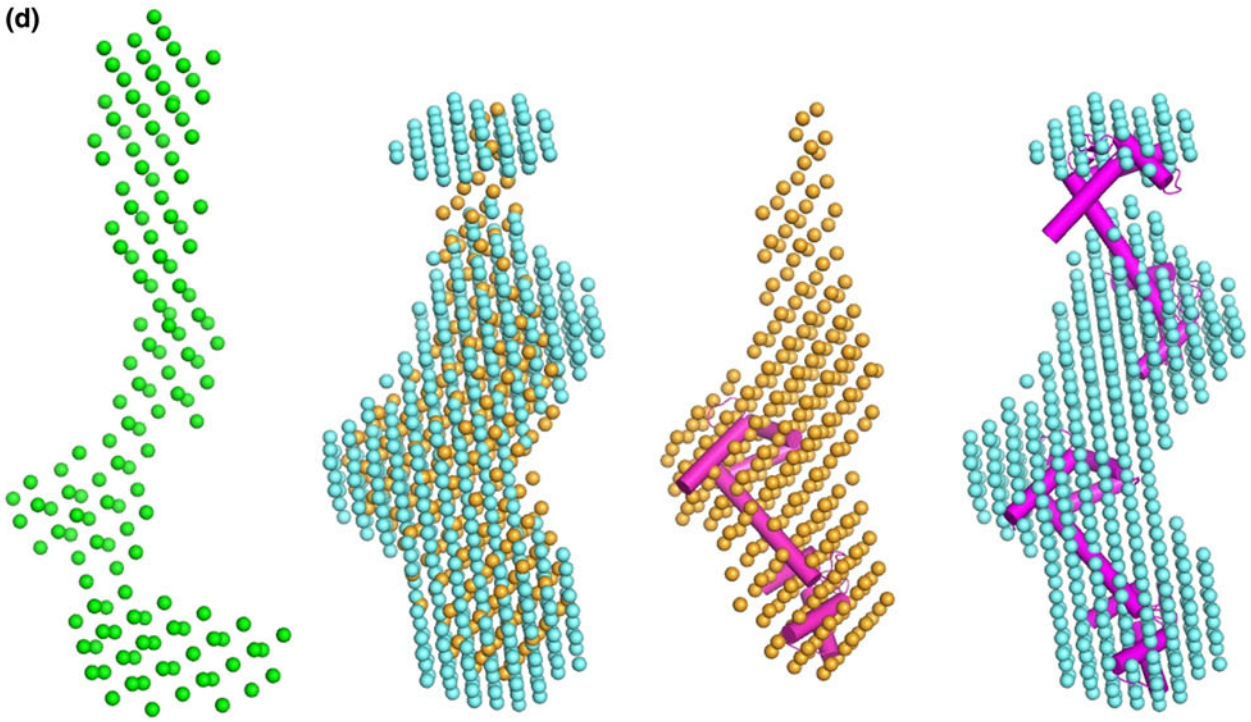
(d)

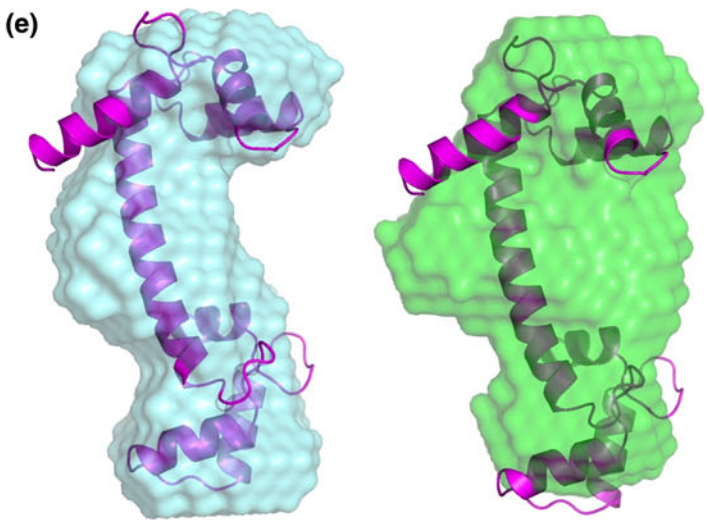
(e)

◀ **Fig. 3** Determination of 3D solution structures. **a** Scattering data of pMBP (*gray dots*), CaM (*green dots*), 1:1 pMBP:CaM (*blue dots*) and 1:2 pMBP:CaM (*red dots*). The fits of the models are displayed as black lines. **b** Distance distribution functions. The coloring scheme is that used in **a**, except that pMBP is in black. **c** Kratky plots for CaM (*green*) and pMBP (*black*). **d** 3D models. From left to right: model of pMBP (*green*); superposition of the ab initio models for the 1:1 (*orange*) and 1:2 (*blue*) complexes between MBP and CaM; apparent locations of the bound CaM (magenta) in the 1:1 and 1:2 complexes. **e** Solution structure for CaM (*blue*) and the mMBP peptide bound to CaM (*green*). The crystal structure of apo CaM is shown as cartoons

diffuse, and restricted to the perinuclear SC soma and some processes (Fig. 6a), to "mature" myelin sheaths, where MBP is expressed strongly in the compacted myelin membranes and excluded from the non-compacted compartments, such as the Schmidt–Lanterman incisures (Fig. 6d) and paranodal loops of the nodes of Ranvier (not shown).

As expected for a molecule involved in signaling pathways, CaM is also localized in the SC soma and processes during the early stages of establishing the SC/neuron relationship (Fig. 6b). However, although its spatial expression profile is very similar to that of MBP (Fig. 6a-b), the two molecules colocalize very little, if at all, at these stages (Fig. 6c). Surprisingly, CaM is also expressed, albeit relatively weakly, in mature myelin sheaths (Fig. 6e), where it colocalizes clearly with MBP in the compacted myelin membranes (Fig. 6f). CaM also appears to be excluded from the Schmidt–Lanterman incisures, like MBP, but, unlike MBP, it is absent from the compacted membranes immediately bordering the incisures (Fig. 6f′).

Table 2 Results from SAXS analysis

Sample	$I(0)$	R_g (nm)	V_p ($\times 10^4$ Å^3)	D_{max} (nm)	$I(0)$ ratio[a]	Volume ratio[b]
CaM	13.6	2.2	2.9	6.5	1	1
pMBP:CaM (1:1)	15.1	3.7	9.0	13	1.1	3.1
pMBP:CaM (1:2)	37.3	3.8	12.6	14	2.7	4.3
CaM + peptide	14.5	1.9	3.1	6	1.1	1.1
pMBP	17.9	5.4	8.7	16	1.3	3.0

The larger than expected volume for pMBP can be explained by its highly disordered nature

[a] Calculated from $I(0)$, comparing to CaM

[b] Calculated from volume, comparing to CaM

Discussion

We used full-length MBP from brain to accurately characterize its interactions with CaM in structural and biophysical terms, for the first time being able to build an experimental 3D model for a full-length protein–protein complex involving MBP, an intrinsically disordered protein. The earliest reports of an interaction between MBP

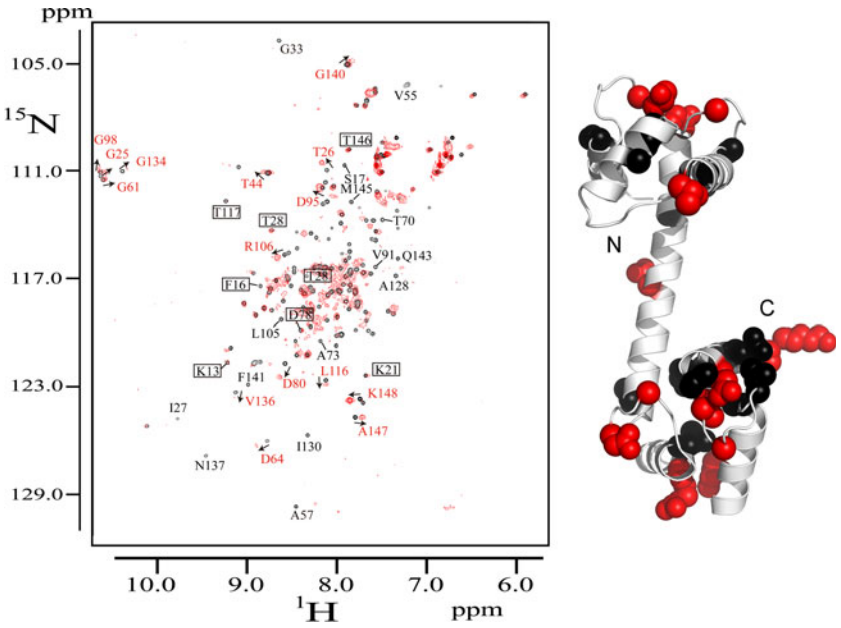

Fig. 4 NMR analysis of labeled CaM in the presence and absence of bMBP. *Left*: Overlay of ^{1}H-^{15}N HSQC spectra of uniformly ^{15}N-labeled Ca^{2+}/CaM alone (*black*) and uniformly ^{15}N-labeled Ca^{2+}/CaM-unlabeled MBP complex (*red*). The samples contained 0.1 mM CaM, 120 mM NaCl, 2.5 mM $CaCl_2$, and 50 mM deuterated Tris–HCl (pH 7.5) in 90% H_2O and 10% D_2O. Changes in cross-peak positions were quantified by $[(\Delta^{15}N_{Hz})^2 + (\Delta^{1}H_{Hz})^2]^{1/2}$. Cross-peaks showing large shifts and disappearance are shown in *red* and *black characters*, respectively; only peaks assigned exactly have been used for the purpose. Cross-peaks showing no shifts are boxed. *Right*: the residues showing large shifts (*red*) or disappearance (*black*) have been mapped onto the structure of CaM

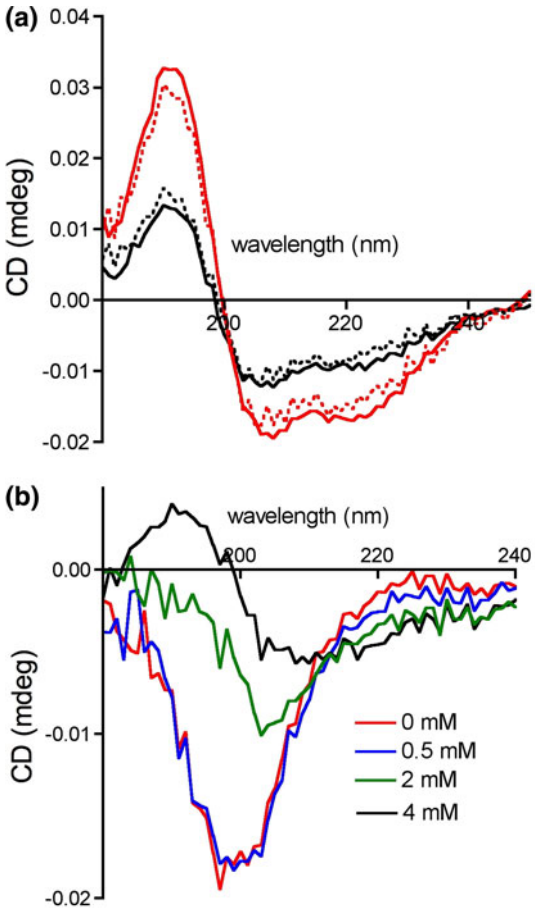

Fig. 5 SRCD analysis of the pMBP–CaM complex and zinc-bound pMBP. In both graphs, raw unsmoothed data are shown; fluctuations result from rather low concentration and photon flux. **a** SRCD spectra of the 1:1 (*black*) and 1:2 (*red*) MBP–CaM complexes. The *dashed lines* indicate the corresponding summation spectra calculated from the separately measured components, i.e., pMBP and CaM. **b** SRCD spectra of pMBP titrated with zinc acetate

and CaM date back to the early 1980s (Barylko and Dobrowolski 1984; Grand and Perry 1980; Iwasa et al. 1981), but relevant structural data on the interaction have been published only recently; the MBP samples used in these studies were synthetic peptides (Majava et al. 2008b) or recombinant His-tagged proteins (Libich and Harauz 2008). The presence of two binding sites for CaM on MBP (Libich et al. 2003b), as well as the IDP nature of MBP (Harauz et al. 2004; Krigbaum and Hsu 1975), have brought about difficulties for structural studies. A recent NMR study shed the first real light on the structural features of the MBP–CaM interaction (Libich and Harauz 2008).

CaM is the most prominent calcium sensor in eukaryotic cells, regulating target proteins, and ultimately transducing the initial Ca^{2+} signal into a wide range of cellular events and processes. Thus, CaM might be a regulatory element of the putative signaling and other physiological roles of MBP in vivo (Boggs and Rangaraj 2000; Boggs et al. 2005; Boggs et al. 2006). Regulation of protein–membrane interactions by CaM has been suggested previously both for MBP and a protein with similar properties, MARCKS (Arbuzova et al. 1998; Boggs and Rangaraj 2000; Harauz et al. 2000; McLaughlin et al. 2005). It is possible that CaM binding regulates the binding of MBP to the myelin membrane and other ligands. MBP is highly positively charged, with pI in the range of 11 (depending on the isoform), and CaM binding (CaM has a calculated pI of 4.1) is expected to neutralize this charge and affect any electrostatic interactions. The predicted CaM-binding sites on MBP are also the regions predicted to be partially membrane-embedded in the context of the tightly packed myelin sheath (Harauz and Libich 2009). It is noteworthy that our preparation of MPEs from rat brain contained CaM, and that MBP is the quantitatively major CaM ligand in white matter. Thus, it can be speculated that CaM binding, dependent on calcium, could regulate the insertion of MBP into compact myelin during myelin formation. In this respect, it is also of interest that solid-state NMR studies have indicated that the C-terminal region of MBP is relatively mobile in its membrane-associated form (Zhong et al. 2007), and could, thus, be accessible for interaction with CaM. The fact that CaM colocalized with MBP in compact myelin clearly warrants further studies on the role of CaM in myelin compaction.

We detected a number of PTMs in rat brain MBP, including glucosylation of Asn82 and Asn90. To our knowledge, this is the first report of glucosylation of MBP; interestingly, glucosylated peptides have been developed over the recent years with mainly diagnostic aims for multiple sclerosis (Carotenuto et al. 2008; Lolli et al. 2005). The glycosylation of MBP in vitro, by UDP-*N*-acetyl-D-galactosamine, has been reported to occur on Thr95 and Thr98 of human MBP (Persaud et al. 1988). Both of these residues have also previously been characterized as MAP kinase phosphorylation targets (Atkins et al. 1999; Boggs et al. 2006; Hirschberg et al. 2003); it is, thus, of interest that the second most abundant protein pulled down from human white matter with CaM affinity chromatography is a MAP kinase, p42MAPK. The kinase is most likely bound to MBP and thus observed in the eluate. In this sense, it is important to note that PLP, MBP, S-MAG, and p42MAPK have been characterized to form a complex in Triton X-100 extracts of CNS myelin (Arvanitis et al. 2002), and that the p38MAPK has been shown to be essential for CNS myelination (Fragoso et al. 2007).

While MBP is one of the key examples of IDPs, a wealth of evidence has accumulated on a possible ligand- or environment-induced local folding of the protein (Ahmed et al. 2009; Chao and Einstein 1970; Haas et al. 2004; Harauz et al. 2004; Mendz et al. 1992; Mendz et al.

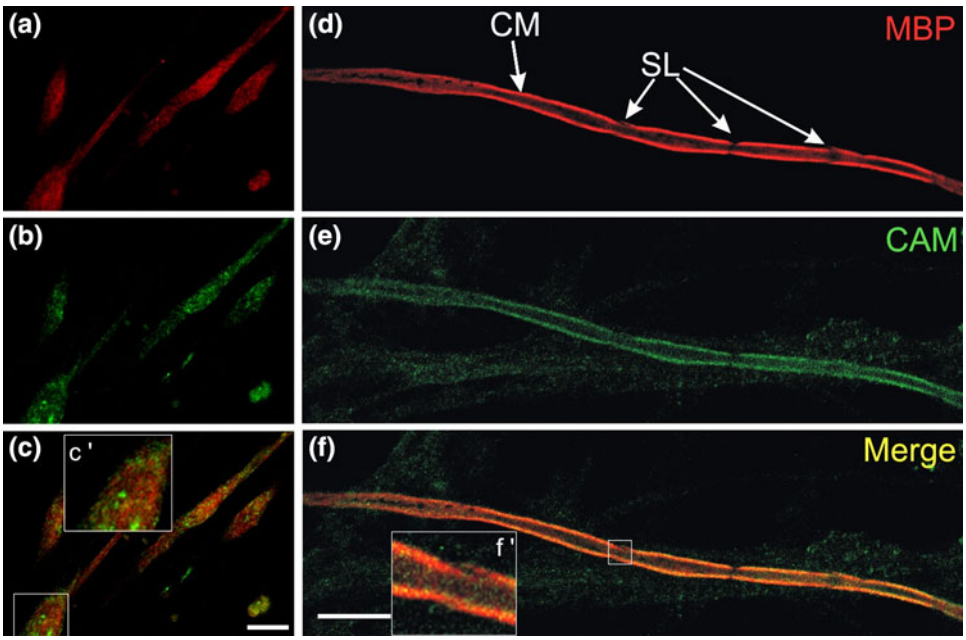

Fig. 6 Immunolocalization of CaM and MBP in myelinating SC/DRG neuron cocultures. SCs and DRGs were cocultured under myelination-permissive conditions for 3 weeks, fixed, double-immunolabelled with anti-MBP (*red*) and anti-CaM (*green*) antibodies, and examined by confocal fluorescence microscopy. Scale bars: 10 μm. Panels **a**–**c**: In pre-myelinating SCs associating with neuronal processes, MBP (*red*, panel **a**) and CaM (*green*, panel **b**) colocalize only weakly, if at all (merged image, panel **c**). The inset (**c**') is a digitally magnified image of the boxed area in panel **c**: note the quasi-total segregation of the *red* and *green* label illustrating the lack of colocalization in the SC soma. Panels **d**–**f**: In mature myelin, MBP (*red*, panel b) and CaM (*green*, panel **e**) colocalize (*yellow*, panel **f**) in compacted myelin membranes (CM) and both are excluded from Schmidt–Lanterman incisures (SL). The inset (**f**') is a digitally magnified image of the boxed area in panel **f**, showing a Schmidt–Lanterman incisure and illustrating the presence of MBP in, and the absence of CaM from, the membranes bordering the incisure

1995; Polverini et al. 1999). Most of such studies have concerned the interaction of MBP, or peptides thereof, with membranes or micelles. Our SAXS and SRCD data indicate that overall, MBP does not contain significant amounts of folded secondary structure when complexed with CaM. In a recent NMR study, conformational changes in MBP were observed in the presence of CaM (Libich and Harauz 2008); these changes involved, however, both the loss and gain of propensity for secondary structure formation. It is, indeed, possible that conformational changes occur in MBP and/or CaM, which neutralize the effect of each other as far as secondary structure content is concerned, when measured by CD spectroscopy.

MBP is also known to bind zinc, and the role of this interaction is assumed to lie in tightening the interaction between MBP and the inner membrane leaflet, aiding myelin compaction (Berlet et al. 1994; Cavatorta et al. 1994; Nuzzo et al. 2002; Riccio et al. 1995; Tsang et al. 1997). Zinc deficiency also may lead to neurological diseases of neuronal origin (Whittle et al. 2009). Our SRCD titration data intriguingly show that, above a certain threshold of zinc concentration, MBP starts to acquire α-helical structure. Further structural studies should elucidate the interplay at the molecular level between MBP, zinc, and the membrane.

To conclude, as evidenced by our structural and biophysical analyses of the complex between full-length CaM and MBP, upon binding two CaM molecules, MBP remains extended and CaM does not collapse. The interaction may also be affected by the wealth of PTMs that have been characterized for MBP. The high binding affinity and colocalization in myelin sheaths indicate a possible function for the CaM–MBP interaction also in vivo.

Acknowledgments This study was supported by the Academy of Finland, the Sigrid Juselius Foundation, the Finnish MS Foundation, the Finnish Cultural Foundation, and the Department of Biochemistry, University of Oulu. Data collection at MAX-Lab and BESSY (project BESSY-09.1.80843) was supported by the European Community-Research Infrastructure Action under the FP6 "Structuring the European Research Area" Programme, contract RII3-CT-2004-506008 (IA-SFS). We thank the staff of beamline I711 at MAX-Lab and the Biocenter Oulu Proteomics core facility for excellent support. The authors declare no conflicts of interest.

References

Ahmed MA, Bamm VV, Shi L, Steiner-Mosonyi M, Dawson JF, Brown L, Harauz G, Ladizhansky V (2009) Induced secondary structure and polymorphism in an intrinsically disordered structural linker of the CNS: solid-state NMR and FTIR

spectroscopy of myelin basic protein bound to actin. Biophys J 96:180–191
Arbuzova A, Murray D, McLaughlin S (1998) MARCKS, membranes, and calmodulin: kinetics of their interaction. Biochim Biophys Acta 1376:369–379
Arvanitis DN, Yang W, Boggs JM (2002) Myelin proteolipid protein, basic protein, the small isoform of myelin-associated glycoprotein, and p42MAPK are associated in the Triton X-100 extract of central nervous system myelin. J Neurosci Res 70:8–23
Atkins CM, Yon M, Groome NP, Sweatt JD (1999) Regulation of myelin basic protein phosphorylation by mitogen-activated protein kinase during increased action potential firing in the hippocampus. J Neurochem 73:1090–1097
Baer AS, Syed YA, Kang SU, Mitteregger D, Vig R, Ffrench-Constant C, Franklin RJ, Altmann F, Lubec G, Kotter MR (2009) Myelin-mediated inhibition of oligodendrocyte precursor differentiation can be overcome by pharmacological modulation of Fyn-RhoA and protein kinase C signalling. Brain 132:465–481
Barylko B, Dobrowolski Z (1984) Ca2+-calmodulin-dependent regulation of F-actin-myelin basic protein interaction. Eur J Cell Biol 35:327–335
Bates IR, Matharu P, Ishiyama N, Rochon D, Wood DD, Polverini E, Moscarello MA, Viner NJ, Harauz G (2000) Characterization of a recombinant murine 18.5-kDa myelin basic protein. Protein Expr Purif 20:285–299
Benjamins JA, Morell P (1978) Proteins of myelin and their metabolism. Neurochem Res 3:137–174
Berlet HH, Bischoff H, Weinhardt F (1994) Divalent metals of myelin and their differential binding by myelin basic protein of bovine central nervous system. Neurosci Lett 179:75–78
Boggs JM (2006) Myelin basic protein: a multifunctional protein. Cell Mol Life Sci 63:1945–1961
Boggs JM, Rangaraj G (2000) Interaction of lipid-bound myelin basic protein with actin filaments and calmodulin. Biochemistry 39:7799–7806
Boggs JM, Rangaraj G, Hill CM, Bates IR, Heng YM, Harauz G (2005) Effect of arginine loss in myelin basic protein, as occurs in its deiminated charge isoform, on mediation of actin polymerization and actin binding to a lipid membrane in vitro. Biochemistry 44:3524–3534
Boggs JM, Rangaraj G, Gao W, Heng YM (2006) Effect of phosphorylation of myelin basic protein by MAPK on its interactions with actin and actin binding to a lipid membrane in vitro. Biochemistry 45:391–401
Brokx RD, Lopez MM, Vogel HJ, Makhatadze GI (2001) Energetics of target peptide binding by calmodulin reveals different modes of binding. J Biol Chem 276:14083–14091
Carotenuto A, Alcaro MC, Saviello MR, Peroni E, Nuti F, Papini AM, Novellino E, Rovero P (2008) Designed glycopeptides with different beta-turn types as synthetic probes for the detection of autoantibodies as biomarkers of multiple sclerosis. J Med Chem 51:5304–5309
Cavatorta P, Giovanelli S, Bobba A, Riccio P, Szabo AG, Quagliariello E (1994) Myelin basic protein interaction with zinc and phosphate: fluorescence studies on the water-soluble form of the protein. Biophys J 66:1174–1179
Cerenius Y, Stahl K, Svensson LA, Ursby T, Oskarsson A, Albertsson J, Liljas A (2000) The crystallography beamline I711 at MAX II. J Synchrotron Radiat 7:203–208
Chao LP, Einstein ER (1970) Physical properties of the bovine encephalitogenic protein; molecular weight and conformation. J Neurochem 17:1121–1132
Dobrowolski Z, Osinska H, Mossakowska M, Barylko B (1986) Ca2+-calmodulin-dependent polymerization of actin by myelin basic protein. Eur J Cell Biol 42:17–26
Dyson HJ, Wright PE (2002) Insights into the structure and dynamics of unfolded proteins from nuclear magnetic resonance. Adv Protein Chem 62:311–340
Fragoso G, Haines JD, Roberston J, Pedraza L, Mushynski WE, Almazan G (2007) p38 mitogen-activated protein kinase is required for central nervous system myelination. Glia 55:1531–1541
Garbay B, Fournier M, Sallafranque ML, Muller S, Boiron F, Heape A, Cassagne C, Bonnet J (1988) Po, MBP, histone, and DNA levels in sciatic nerve. Postnatal accumulation studies in normal and trembler mice. Neurochem Pathol 8:91–107
Garbay B, Heape AM, Sargueil F, Cassagne C (2000) Myelin synthesis in the peripheral nervous system. Prog Neurobiol 61:267–304
Grand RJ, Perry SV (1980) The binding of calmodulin to myelin basic protein and histone H2B. Biochem J 189:227–240
Haas H, Oliveira CL, Torriani IL, Polverini E, Fasano A, Carlone G, Cavatorta P, Riccio P (2004) Small angle X-ray scattering from lipid-bound myelin basic protein in solution. Biophys J 86:455–460
Harauz G, Libich DS (2009) The classic basic protein of myelin-conserved structural motifs and the dynamic barcode involved in membrane adhesion and protein–protein interactions. Curr Protein Peptide Sci 10:196–215
Harauz G, Ishiyama N, Bates IR (2000) Analogous structural motifs in myelin basic protein and in MARCKS. Mol Cell Biochem 209:155–163
Harauz G, Ishiyama N, Hill CM, Bates IR, Libich DS, Fares C (2004) Myelin basic protein-diverse conformational states of an intrinsically unstructured protein and its roles in myelin assembly and multiple sclerosis. Micron 35:503–542
Hill CM, Harauz G (2005) Charge effects modulate actin assembly by classic myelin basic protein isoforms. Biochem Biophys Res Commun 329:362–369
Hirschberg D, Radmark O, Jornvall H, Bergman T (2003) Thr94 in bovine myelin basic protein is a second phosphorylation site for 42-kDa mitogen-activated protein kinase (ERK2). J Protein Chem 22:177–181
Homchaudhuri L, Polverini E, Gao W, Harauz G, Boggs J (2009) Influence of membrane surface charge and post-translational modifications to myelin basic protein on its ability to tether the Fyn-SH3 domain to a membrane in vitro. Biochemistry 48:2385–2393
Honkanen H, Lahti O, Nissinen M, Myllylä RM, Kangas S, Päiväläinen S, Alanne MH, Peltonen S, Peltonen J, Heape AM (2007) Isolation, purification and expansion of myelination-competent, neonatal mouse Schwann cells. Eur J Neurosci 26:953–964
Iwasa Y, Iwasa T, Matsui K, Higashi K, Miyamoto E (1981) Interaction of calmodulin with chromatin associated proteins and myelin basic protein. Life Sci 29:1369–1377
Kim JK, Mastronardi FG, Wood DD, Lubman DM, Zand R, Moscarello MA (2003) Multiple sclerosis: an important role for post-translational modifications of myelin basic protein in pathogenesis. Mol Cell Proteomics 2:453–462
Konarev PV, Petoukhov MV, Volkov VV, Svergun DI (2006) ATSAS 2.1, a program package for small-angle scattering data analysis. J Appl Cryst 39:277–286
Krigbaum WR, Hsu TS (1975) Molecular conformation of bovine A1 basic protein, a coiling macromolecule in aqueous solution. Biochemistry 14:2542–2546
Kursula P (2008) Structural properties of proteins specific to the myelin sheath. Amino Acids 34:175–185
Kursula P, Majava V (2007) A structural insight into lead neurotoxicity and calmodulin activation by heavy metals. Acta Crystallogr Sect F Struct Biol Cryst Commun 63:653–656

Libich DS, Harauz G (2002a) Interactions of the 18.5-kDa isoform of myelin basic protein with Ca(2+)-calmodulin: in vitro studies using fluorescence microscopy and spectroscopy. Biochem Cell Biol 80:395–406

Libich DS, Harauz G (2002b) Interactions of the 18.5 kDa isoform of myelin basic protein with Ca2 + -calmodulin: in vitro studies using gel shift assays. Mol Cell Biochem 241:45–52

Libich DS, Harauz G (2008) Backbone dynamics of the 18.5 kDa isoform of myelin basic protein reveals transient alpha-helices and a calmodulin-binding site. Biophys J 94:4847–4866

Libich DS, Hill CM, Bates IR, Hallett FR, Armstrong S, Siemiarczuk A, Harauz G (2003a) Interaction of the 18.5-kD isoform of myelin basic protein with Ca2+-calmodulin: effects of deimination assessed by intrinsic Trp fluorescence spectroscopy, dynamic light scattering, and circular dichroism. Protein Sci 12:1507–1521

Libich DS, Hill CM, Haines JD, Harauz G (2003b) Myelin basic protein has multiple calmodulin-binding sites. Biochem Biophys Res Commun 308:313–319

Libich DS, Robertson VJ, Monette MM, Harauz G (2004) Backbone resonance assignments of the 18.5 kDa isoform of murine myelin basic protein (MBP). J Biomol NMR 29:545–546

Lolli F, Mulinacci B, Carotenuto A, Bonetti B, Sabatino G, Mazzanti B, D'Ursi AM, Novellino E, Pazzagli M, Lovato L, Alcaro MC, Peroni E, Pozo-Carrero MC, Nuti F, Battistini L, Borsellino G, Chelli M, Rovero P, Papini AM (2005) An N-glucosylated peptide detecting disease-specific autoantibodies, biomarkers of multiple sclerosis. Proc Natl Acad Sci USA 102:10273–10278

Maatta JA, Coffey ET, Hermonen JA, Salmi AA, Hinkkanen AE (1997) Detection of myelin basic protein isoforms by organic concentration. Biochem Biophys Res Commun 238:498–502

Majava V, Loytynoja N, Chen WQ, Lubec G, Kursula P (2008a) Crystal and solution structure, stability and post-translational modifications of collapsin response mediator protein 2. FEBS J 275:4583–4596

Majava V, Petoukhov MV, Hayashi N, Pirila P, Svergun DI, Kursula P (2008b) Interaction between the C-terminal region of human myelin basic protein and calmodulin: analysis of complex formation and solution structure. BMC Struct Biol 8:10

McLaughlin S, Hangyas-Mihalyne G, Zaitseva I, Golebiewska U (2005) Reversible-through calmodulin–electrostatic interactions between basic residues on proteins and acidic lipids in the plasma membrane. Biochem Soc Symp 72:189–198

Mendz GL, Jamie IM, White JW (1992) Effects of acyl chain length on the conformation of myelin basic protein bound to lysolipid micelles. Biophys Chem 45:61–77

Mendz GL, Miller DJ, Ralston GB (1995) Interactions of myelin basic protein with palmitoyllysophosphatidylcholine: characterization of the complexes and conformations of the protein. Eur Biophys J 24:39–53

Nuzzo S, Meneghini C, Mobilioo S, Haas H, Riccio P, Fasano A, Cavatorta P, Morante S (2002) An X-ray absorption spectroscopy study of the zinc environment in Langmuir–Blodgett phospholipid multilayers. Biophys J 83:3507–3512

Oakberg TC, Trunk JG, Sutherland JC (2000) Calibration of photoelastic modulators in the vacuum UV. Proc SPIE 4133:101–110

Päiväläinen S, Nissinen M, Honkanen H, Lahti O, Kangas SM, Peltonen J, Peltonen S, Heape AM (2008) Myelination in mouse dorsal root ganglion/Schwann cell cocultures. Mol Cell Neurosci 37:568–578

Persaud R, Fraser P, Wood DD, Moscarello MA (1988) The glycosylation of human myelin basic protein at threonines 95 and 98 occurs sequentially. Biochim Biophys Acta 966:357–361

Polverini E, Fasano A, Zito F, Riccio P, Cavatorta P (1999) Conformation of bovine myelin basic protein purified with bound lipids. Eur Biophys J 28:351–355

Polverini E, Rangaraj G, Libich DS, Boggs JM, Harauz G (2008) Binding of the proline-rich segment of myelin basic protein to SH3 domains: spectroscopic, microarray, and modeling studies of ligand conformation and effects of posttranslational modifications. Biochemistry 47:267–282

Reichardt G, Noll T, Packe I, Rotter P, Schmidt JS, Gudat W (2001) Adaption of the BESSY I-3 m normal incidence monochromators to the BESSY II source. Nucl Inst Method Phys Res A 467:458–461

Riccio P, Giovannelli S, Bobba A, Romito E, Fasano A, Bleve-Zacheo T, Favilla R, Quagliariello E, Cavatorta P (1995) Specificity of zinc binding to myelin basic protein. Neurochem Res 20:1107–1113

Spyranti Z, Tselios T, Deraos G, Matsoukas J, Spyroulias GA (2009) NMR structural elucidation of myelin basic protein epitope 83-99 implicated in multiple sclerosis. Amino Acids, in press

Sutherland JC (1996) Circular dichroism using synchrotron radiation. In: Fasman GD (ed) Circular dichroism and the conformational analysis of biomolecules. Plenum Press, New York, pp 599–633

Tsang D, Tsang YS, Ho WK, Wong RN (1997) Myelin basic protein is a zinc-binding protein in brain: possible role in myelin compaction. Neurochem Res 22:811–819

Tselios T, Probert L, Kollias G, Matsoukas E, Roumelioti P, Alexopoulos K, Moore GJ, Matsoukas J (1998) Design and synthesis of small semi-mimetic peptides with immunomodulatory activity based on myelin basic protein (MBP). Amino Acids 14:333–341

Whittle N, Lubec G, Singewald N (2009) Zinc deficiency induces enhanced depression-like behaviour and altered limbic activation reversed by antidepressant treatment in mice. Amino Acids 36:147–158

Zand R, Li MX, Jin X, Lubman D (1998) Determination of the sites of posttranslational modifications in the charge isomers of bovine myelin basic protein by capillary electrophoresis-mass spectroscopy. Biochemistry 37:2441–2449

Zhong L, Bamm VV, Ahmed MA, Harauz G, Ladizhansky V (2007) Solid-state NMR spectroscopy of 18.5 kDa myelin basic protein reconstituted with lipid vesicles: spectroscopic characterisation and spectral assignments of solvent-exposed protein fragments. Biochim Biophys Acta 1768:3193–3205